UC San Diego
UC San Diego Previously Published Works

Title

Dysfunctional Autism Risk Genes Cause Circuit-Specific Connectivity Deficits With Distinct Developmental Trajectories

Permalink

https://escholarship.org/uc/item/6d53s1dg

Journal

Cerebral Cortex, 28(7)

ISSN

1047-3211

Authors

Zerbi, Valerio
Ielacqua, Giovanna D
Markicevic, Marija
et al.

Publication Date

2018-07-01

DOI

10.1093/cercor/bhy046

Peer reviewed

OXFORD

ORIGINAL ARTICLE

Dysfunctional Autism Risk Genes Cause Circuit-Specific Connectivity Deficits With Distinct Developmental Trajectories

Valerio Zerbi [1], Giovanna D. Ielacqua[2], Marija Markicevic[1], Matthias Georg Haberl[3], Mark H. Ellisman[3,4], Arjun A-Bhaskaran[5,6], Andreas Frick[5,6], Markus Rudin[2,7,8] and Nicole Wenderoth[1,7]

[1]Neural Control of Movement Lab, HEST, ETH Zürich, Winterthurerstrasse 190, 8057 Zurich, Switzerland, [2]Institute for Biomedical Engineering, University and ETH Zurich, Wolfgang-Pauli-Str. 27, 8093 Zurich, Switzerland, [3]National Center for Microscopy and Imaging Research, University of California, San Diego, La Jolla, CA 92093, USA, [4]Department of Neurosciences, University of California, San Diego, La Jolla, CA 92093, USA, [5]INSERM, Neurocentre Magendie, Physiopathologie de la Plasticité Neuronale, U1215, 33077 Bordeaux, France, [6]University of Bordeaux, Neurocentre Magendie, Physiopathologie de la Plasticité Neuronale, 33077 Bordeaux, France, [7]Neuroscience Center Zurich, University and ETH Zurich, Winterthurerstrasse 190, 8057 Zurich, Switzerland and [8]Institute of Pharmacology and Toxicology, University of Zurich, Winterthurerstrasse 190, 8057 Zurich, Switzerland

Address correspondence to Dr Valerio Zerbi, Neural Control of Movement Lab, Department of Health Sciences and Technology, ETH Zurich, Winterthurerstrasse 190, 8057 Zuerich, Switzerland. Email: valerio.zerbi@hest.ethz.ch orcid.org/0000-0001-7984-9565

Abstract

Autism spectrum disorders (ASD) are a set of complex neurodevelopmental disorders for which there is currently no targeted therapeutic approach. It is thought that alterations of genes regulating migration and synapse formation during development affect neural circuit formation and result in aberrant connectivity within distinct circuits that underlie abnormal behaviors. However, it is unknown whether deviant developmental trajectories are circuit-specific for a given autism risk-gene. We used MRI to probe changes in functional and structural connectivity from childhood to adulthood in Fragile-X ($Fmr1^{-/y}$) and contactin-associated ($CNTNAP2^{-/-}$) knockout mice. Young $Fmr1^{-/y}$ mice (30 days postnatal) presented with a robust hypoconnectivity phenotype in corticocortico and corticostriatal circuits in areas associated with sensory information processing, which was maintained until adulthood. Conversely, only small differences in hippocampal and striatal areas were present during early postnatal development in $CNTNAP2^{-/-}$ mice, while major connectivity deficits in prefrontal and limbic pathways developed between adolescence and adulthood. These findings are supported by viral tracing and electron micrograph approaches and define 2 clearly distinct connectivity endophenotypes within the autism spectrum. We conclude that the genetic background of ASD strongly influences which circuits are most affected, the nature of the phenotype, and the developmental time course of the associated changes.

Key words: autism, brain connectivity, CNTNAP2, FMR1, resting-state functional MRI

Introduction

Autism spectrum disorders (ASD) are among the most prevalent neurodevelopmental disorders with no currently available cure. While there are a large number of genetic risk factors associated with ASD (Ronald and Hoekstra 2011), only a few genetic variants are causal, as is the case in the neurodevelopmental syndrome Fragile-X (FXS), which has a higher than expected comorbidity with autism. It is critical to note, however, that variations in ASD risk genes do not directly affect behavior. Rather they affect molecular pathways that influence the development of neurons and synapses that, in turn, affect brain connectivity and function at the system level. Defective synaptic function leading to an excitation–inhibition (E/I) imbalance is commonly invoked as one possible explanation for ASD (Rubenstein and Merzenich 2003), and is supported by evidence in humans and rodents (Yizhar et al. 2011; Hashemi et al. 2017; Selimbeyoglu et al. 2017). According to this theory, E/I imbalance affects molecular mechanisms harnessing neuroplasticity, which is essential for brain development and experience-dependent learning at all ages. Early disruptions of E/I balance have been linked to long-lasting alterations in structural and functional connectivity within specific brain circuits, leading to a variety of clinical symptoms in ASD (Courchesne 2002; Belmonte et al. 2004; Vasa et al. 2016). Indeed, many functional magnetic resonance imaging (fMRI) studies have identified aberrant functional connectivity in individuals with ASD (Alaerts et al. 2014, 2015, 2016; Balsters et al. 2016; Balsters, Apps, et al. 2017; Balsters, Mantini, et al. 2017), even when tested during the resting state. However, the regional patterns of ASD-specific hypoconnectivity or hyperconnectivity vary considerably across studies and patient cohorts, suggesting that connectivity examined at a single developmental stage is only a moderate predictor of the pathology (Kassraian-Fard et al. 2016; Abraham et al. 2017). By contrast, a recent imaging study (Hazlett et al. 2017) in ASD infants suggests that aberrant developmental trajectories within circuits underlying abnormal behaviors might be sensitive markers of the disease. Yet to date, no longitudinal study has been performed that compares the developmental trajectory of brain connectivity between ASD and control subjects. This leaves many fundamental questions unanswered: (1) Which factors drive the pathological trajectory? (2) At which developmental stage does abnormal connectivity manifest itself in subjects with ASD? (3) Are certain brain circuits more susceptible to disrupted neural development than others?

We addressed these questions by measuring resting-state connectivity in 2 well-characterized mouse models exhibiting an Autism phenotype, in which E/I imbalance has been linked with both functional connectivity defects and phenotypical ASD-like behavior in adulthood (Haberl, Zerbi, et al. 2015; Garcia-Pino et al. 2017; Lee et al. 2017; Liska et al. 2017; Selimbeyoglu et al. 2017). Specifically, loss of the Fragile X mental retardation protein leads to excessive excitatory compared with inhibitory inputs in the sensory cortical system (Garcia-Pino et al. 2017), while in CNTNAP2 deficient mice a decreased ratio of GABA to glutamate is seen in the medial prefrontal cortex (Selimbeyoglu et al. 2017), a finding paralleling results in autism patients (Harada et al. 2011).

In order to assess how pathological brain connectivity develops from childhood to adulthood, here we used a longitudinal design starting our measurements immediately after weaning. Specifically, we tested the hypothesis that the genetic background is an important factor determining when delayed or abnormal development of brain circuits become manifest in resting state connectivity measurements. We investigate the developmental trajectory of functional and structural connectivity in Fragile X mental retardation 1 knockout (Fmr1$^{-/y}$) and contactin-associated protein 2 knockout (CNTNAP2$^{-/-}$) mice using MRI techniques (Grandjean et al. 2014; Zerbi et al. 2014, 2015). FMR1 plays a pivotal role in early embryotic neurodevelopment (Hinds et al. 1993) whereas the physiological expression of CNTNAP2 begins at around E14 but peaks during adulthood (P56) (Penagarikano et al. 2011). Because of the divergent expression profile of these 2 genes, we hypothesized that the emergence of circuit deficits would become apparent at different developmental stages: we expected to find strong differences in Fmr1$^{-/y}$ mice compared with wildtype littermates during childhood, whereas CNTNAP2$^{-/-}$ are expected to exhibit connectivity abnormalities at a later age.

Materials and Methods

Mice

All experiments were performed in accordance with the Swiss federal guidelines for the use of animals in research, and under licensing from the Zürich Cantonal veterinary office. Second-generation Fmr1 knockout (Fmr1$^{-/y}$) (Mientjes et al. 2006) and CNTNAP2$^{-/-}$ strains (Jackson laboratory, Maine, USA) were bred at the ETH animal facility (EPIC, Zürich, Switzerland) and kept on C57Bl/6j background for at least 6 generations. Animals were caged in standard housing, with food and water ad libitum, and a 12 h day/night cycle. The experimenter was blind to the genotype for all experiments. Only male Fmr1 mice were used, consistent with previous studies on this mouse model. In addition, the FMR1 gene, which is impaired in the human disorder, is carried on the X-chromosome leading to a strong penetrance of the mutation in males. Due to the random nature of the X-chromosome inactivation, females are mosaic rather than homozygous, which leads to a more subtle manifestation of symptoms (Hagerman and Hagerman 2016).

Magnetic Resonance Imaging

Fmr1$^{-/y}$ and CNTNAP2$^{-/-}$ mice were longitudinally evaluated during early development (juvenile stage: 34 ± 4 days postnatal, young-adult stage: 58 ± 5 days postnatal, adult stage: 112 ± 11 days postnatal). There was no difference in age and bodyweight between groups at each time point. Data acquisition was performed on a Biospec 70/16 small animal MR system (Bruker BioSpin MRI, Ettlingen, Germany) with a cryogenic quadrature surface coil (Bruker BioSpin AG, Fällanden, Switzerland). A standard gradient-echo echo planar imaging sequence (GE-EPI, repetition time TR = 1000 ms, echo time TE = 15 ms, in-plane resolution RES = 0.22×0.2 mm^2, number of slice NS = 20, slice thickness ST = 0.4 mm, slice gap SG = 0.1 mm) was applied to acquire 2000 volumes in 38 min. In addition, we acquired anatomical T2-weighted images (FLASH sequence, in-plane resolution of 0.05×0.02 mm^2, TE = 3.51, TR = 522 ms) and diffusion weighted images (DWI, multi-shot SE-EPI sequence, 4 segments, TR = 2000 ms, TE = 22 ms, RES = 0.2×0.2 mm^2, NS = 28, ST = 0.4 mm, SG = 0 mm, b-values = 1000–2000 s/mm^2, 90 directions encoding, for a total scan time of 18 min). The levels of anesthesia and mouse physiological parameters were monitored following an established protocol to obtain a reliable measurement of functional connectivity (Zerbi et al. 2015) (see Supplementary Material for details).

Data Preprocessing and Statistics

Rs-fMRI

Resting state fMRI datasets were preprocessed using an existing pipeline for removal of unwanted confounds from the time series (Zerbi et al. 2015), with modifications (Sethi et al. 2017). After artifact removal (see Supplementary Material) and de-spiking (Patel et al. 2014), datasets were band-pass filtered (0.01–0.3 Hz), coregistered to the skull-stripped T2-weighted images and normalized to the AMBMC template (www.imaging.org.au/AMBMC) using ANTs v2.1 (picsl.upenn.edu/ANTS).

Diffusion Tensor Parameter Estimation

After individual realignment of the diffusion images, eddy current correction and tensor estimation was performed (for further details, see Zerbi et al. 2013), then fractional anisotropy (FA) and mean diffusivity (MD) maps were calculated (see Supplementary Material). The resulting volumes were spatially normalized to the AMBMC template.

Transmission Electron Microscopy

After careful tissue preparation (see Supplementary Material) areas of interest from the corpus callosum were isolated and mounted onto dummy acrylic blocks with cyanoacrylic adhesive. Ultrathin sections (70 nm thick) were prepared using an ultramicrotome. Electron micrographs were recorded using a FEI Spirit transmission electron microscope operated at 120 kV.

Retrograde Tracing Using Glycoprotein-Deleted Rabies Virus

Virus Production

SAD ΔG-mCherry (a kind gift from Prof. K.-K. Conzlemann, Ludwig-Maximillian University, Munich) pseudotyped with its native glycocoprotein was amplified and purified as described previously by Haberl, Viana da Silva, et al. (2015).

Stereotaxic Injections and Slice Preparation

Sterotaxic injections were performed in 12-week-old Fmr1$^{-/y}$ and wildtype littermate mice using protocols approved by the Ethics Committee of Bordeaux (CE50). Purified viral particles were injected in the right caudate putamen (stereotactic coordinates with respect to Bregma: –0.88 mm anterior/posterior, +3 mm lateral/medial). Injections of 500 nL each were performed at 2 positions dorsal/ventral: –2.8 and –3 mm (with respect to pia). Injection volume and rate of injection (50 nL/min) were monitored using an Ultra Micro Pump (World Precision Instruments) as described in Haberl et al. (2017). Mice were perfused after a week of injection and the brains were sectioned as described by Haberl, Viana da Silva, et al. (2015).

Fluorescence Microscopy and Analysis

Red fluorescent protein (mCherry) expression in neurons at various brain regions were used to quantify the projection density. We used a scanning mosaic wide-field fluorescence acquisition system (NanoZoomer, Hamamatsu) equipped with a 20 × 0.75 numerical aperture objective to acquire the images. Images were arranged using the mouse brain atlas (Allen Brain Atlas). We used NDP.view2 (Hamamatsu) and manually counted 46 467 neurons labeled with the red fluorescent protein and further plotted them into different groups according to the genotype and brain areas.

Results

Using a longitudinal design, we compared 2 knockout mouse strains, Fmr1$^{-/y}$ ($n = 13$) and CNTNAP2$^{-/-}$ ($n = 14$) to their own control littermates (Fmr1$^{+/y}$: $n = 12$, CNTNAP2$^{+/+}$: $n = 12$), at 3 different stages of postnatal development, p32 (juvenile), p58 (young adult) and p112 (adult). Both males and females CNTNAP2 mice were included in the study, whilst heterozygous mice were excluded. Overall, CNTNAP2 males and females were similarly distributed between subgroups (CNTNAP2$^{-/-}_{females}$ = 5; CNTNAP2$^{+/+}_{females}$ = 5; CNTNAP2$^{-/-}_{males}$ = 9; CNTNAP2$^{+/+}_{males}$ = 7). The differences in bodyweight between males and females at each age-point were not significant ($P = 0.524$) and both groups showed a significant increase in bodyweight over time ($P = 0.001$). Gender was considered as a covariate in all of the following statistical analyses.

Development of Functional Connectivity Networks

We first employed a data-driven independent component analysis (ICA) approach across all animals (124 rs-fMRI datasets) and identified 16 meaningful resting-state networks (RSNs), which were named according to the ontological area of their maximum Z-score intensity (Fig. 1). For each of these RSN, we estimated a surrogate measure coupling strength at the voxel level using a dual regression approach (Filippini et al. 2009). We found an overall genotype effect: Fmr1$^{-/y}$ mice differed from their wildtype littermates mainly in lateral striatum and auditory/associative cortical networks. The only differences between CNTNAP2$^{-/-}$ and control littermates were found in small clusters in the ventral striatum and ventral hippocampus (Fig. 2A–C).

Next, we derived an index of coupling strength at the network level by averaging the Z-scores from the group-mean RSN masks (threshold at the 75th percentile, Fig. 1B) to identify interactions between genotype and developmental trajectories. Irrespective of their age, Fmr1$^{y/-}$ mice exhibited reduced network coupling compared with controls (Genotype main effect) in the dorsolateral striatum ($P_{FDR} = 0.016$) and the auditory/associative network ($P_{FDR} = 0.016$) throughout postnatal development (Fig. 2B). By contrast, for CNTNAP2$^{-/-}$ mice we observed a significant genotype × age interaction ($P_{FDR} = 0.038$) in the ventral striatum indicative of a deviation from the developmental trajectory. Pairwise comparisons showed that this effect is driven by an increase in network strength during adulthood in CNTNAP2$^{-/-}$ mice (postnatal day, p112). In line with the results at the voxel level, we observed an overall reduction in ventral hippocampus connectivity strength, although it did not survive FDR correction ($P_{FDR} = 0.062$) (Fig. 2D).

Development of Functional Connectome

To further probe which specific functional connections showed group differences we used a network-based statistics method (NBS) (Zalesky et al. 2010). Briefly, BOLD time series were extracted using the Allen Reference Atlas ontology (Oh et al. 2014) and their connectivity couplings were measured using regularized Pearson's correlation coefficients (FSLNets). Only macroareas that were fully covered by the field of view used for rs-fMRI acquisition were included in the analysis (isocortex, hippocampal formation, cortical subplate, striatum, pallidum, thalamus, hypothalamus, and midbrain) and consisted of 65 ROIs in each hemisphere. In order to remove spurious connections from the NBS analysis, matrices were given an arbitrary sparsity threshold, retaining only the top-10% of connections
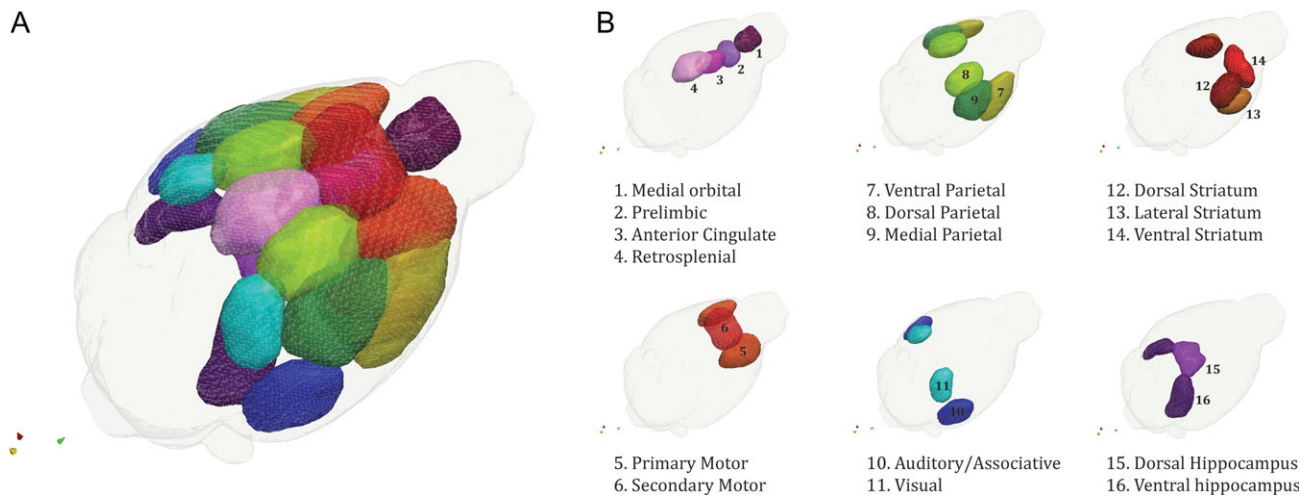
Figure 1. Selected brain networks. From a group-level independent component analysis of all our 124 resting-state fMRI datasets we selected 16 meaningful networks, many of which bear a striking resemblance to analogous human networks underscoring the high translational value of rs-fMRI across different species. Brain networks are overlaid with an anatomical template in a graphical 3D representations (A) and split according to their macroscopic ontology (B).

(Supplementary Fig. S1). A general linear model was used to model overall genotype differences, and genotype × age interactions. Permutation testing, using unpaired t-tests, was performed with 5000 permutations. A test statistic was then computed for each connection and a threshold applied ($t = 2.3$) to produce a set of suprathreshold connections, thereby identifying anatomical networks that show significant differences in structural connectivity between groups.

In Fmr1$^{-/y}$ mice, permutation testing for genotype differences identified one large and symmetric network with reduced coupling strength ($P = 0.033$). This network comprises bilateral sensory-related cortices, caudoputamen (CP), insula, and amygdala. These differences were seen in both juvenile and adult mice, confirming our original hypothesis that in Fmr1$^{-/y}$ mice functional connectivity deficits occur within 30 days of birth (Fig. 3A). To provide a plausible anatomical cause for these functional results, we injected retrograde viral tracer into the CP of Fmr1$^{-/y}$ mice and found that projections from somatosensory cortices, agranular insular, and visceral cortices were reduced by up to ~25% compared with wildtype littermates (Supplementary Fig. S2). These results strongly suggest that in Fmr1$^{-/y}$ mice, the reduced functional connectivity within the somatosensory RSN is directly coupled with a loss of long-range anatomical connections.

In CNTNAP2$^{-/-}$ mice, several genotype × age interactions were found. Specifically, at p112 3 networks showed significantly reduced functional connectivity (Fig. 3B). The first mainly involves connections from the anterior cingulate cortex (ACA) to other prefrontal cortical areas (prelimbic, Infralimbic, and orbitofrontal), retrosplenial cortices and superior colliculus (N1, $P = 0.015$). Interestingly a similar reduction in functional coupling between these regions was also observed by Liska and colleagues in adult CNTNAP2$^{-/-}$ mice, which highlight the strength and reproducibility of rs-fMRI phenotyping to characterize connectivity deficits in this model. Reduced neural projections in the cingulate cortex were also observed (Liska et al. 2017), suggesting a contribution of defective mesoscale axonal wiring to the observed functional impairments.

A reduction of connectivity during adulthood (p112) was also seen in a network comprising the right entorhinal cortex (ENT), temporal association area (TEa), presubiculum (PRE) and

perirhinal areas (PERI) (N2, $P = 0.026$), and in several nodes of the ventral hippocampus (N3, $P = 0.026$). All these results were confirmed by mixed-model statistics, using the averaged network strength as a dependent variable. The only overall genotype difference, regardless of age, was driven by increased coupling strength in one symmetric network located in the ventral striatum (N4, $P = 0.001$). This network included bilateral nucleus accumbens (ACB), pallidum (PAL), hypothalamus (HY), thalamus (polymodal association cortex related, DORpm) and fundus of the striatum (FS). Mixed-model analysis of this network revealed an age-dependent effect, with the strongest deviation from the wildtype values seen during adulthood (Fig. 3C).

Development of Structural Connectivity

Structural integrity of major axon bundles was quantified by extracting FA values from 7 major white matter structures identified by the Allen Mouse Brain atlas (Fig. 4). All white matter tracts exhibited a marked increase in FA values with age ($P_{FDR} < 0.01$), which was independent of genotype and possibly reflects increased myelination and coherent alignment of fiber bundles during development (Lebel et al. 2008).

However, similar to previous human and rodent studies (Hashimoto et al. 2011; Haberl, Zerbi, et al. 2015), we found a marked FA reduction in Fmr1$^{-/y}$ mice compared with wildtype at all time points in the anterior commissure ($P_{FDR} < 0.01$), corpus callosum ($P_{FDR} < 0.01$), cingulum ($P_{FDR} = 0.01$) and internal capsule ($P_{FDR} = 0.02$) (Fig. 4B).

CNTNAP2$^{-/-}$ mice deviated from the developmental trajectory of controls during adulthood exhibiting a clear reduction of structural integrity in the cingulum (genotype × age: $P_{FDR} = 0.01$), a white matter tract projecting from the cingulate area to the entorhinal cortex, allowing for communication between components in the limbic system (Fig. 4C). This age-dependent structural abnormality corroborates with the functional connectivity changes observed, thus supporting the idea that both structural and functional deficits in these mice become apparent only later in life, and affect primarily the limbic system. An FA reduction was also observed in the corpus callosum of CNTNAP2$^{-/-}$ mice, but did not survive FDR correction for multiple comparisons ($P = 0.032$, uncorrected).
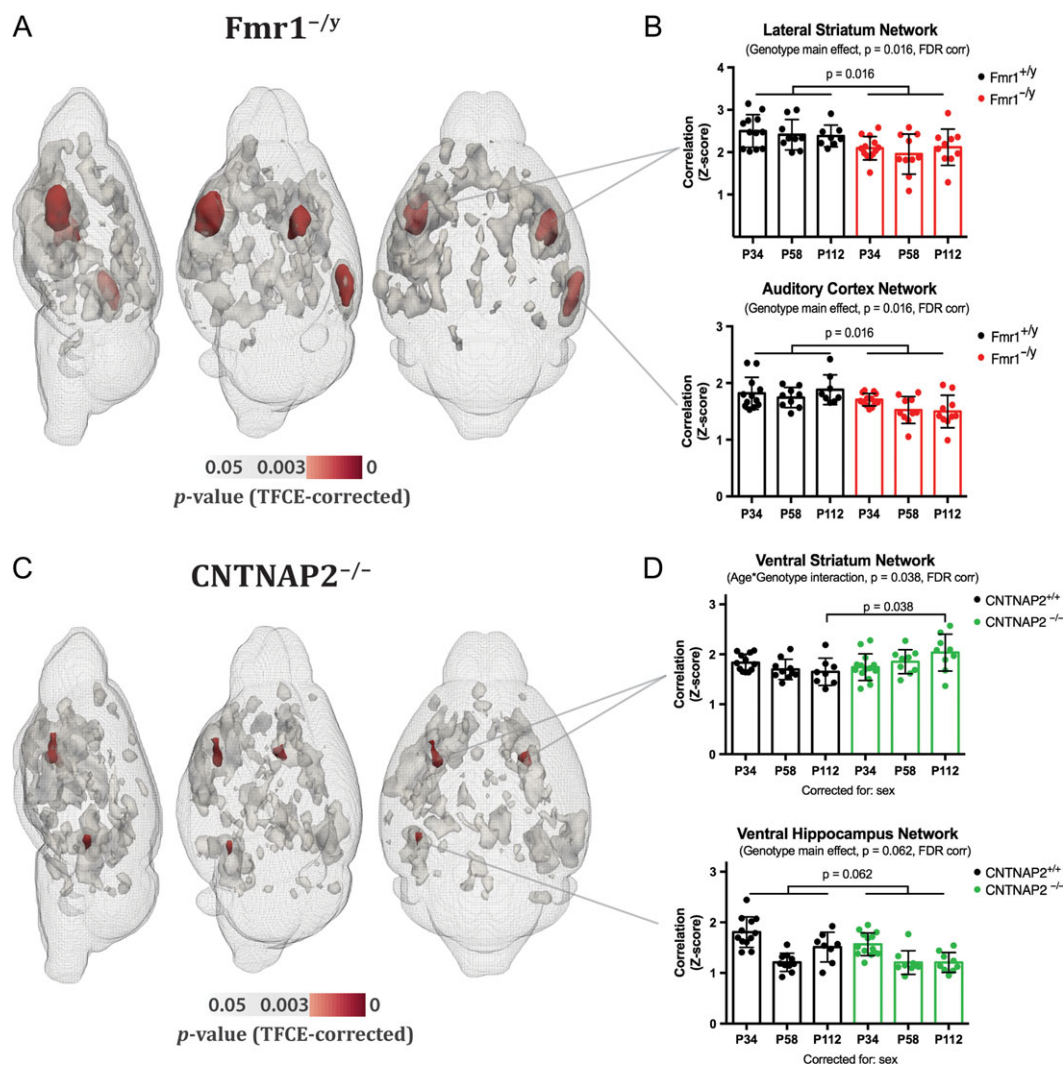
Figure 2. Genotype-dependent differences in resting state network strength.   (A, C) Voxel-wise statistical analyses revealed significant genotype differences in resting-state network strength in both Fmr1$^{-/y}$ and CNTNAP2$^{-/-}$ models (shown in red). Other clusters that represent significant differences in Z-scores but did not survive Bonferroni correction (0.05/16 networks) are shown in gray. (B, D) Mixed linear models showed significant network strength reduction in lateral striatum and auditory/associative cortex in Fmr1$^{-/y}$ mice (for both networks: P$_{FDR}$ = 0.016). A similar reduction was observed in the prelimbic and posterior parietal networks, although it did not reach significance after FDR correction (both networks, P$_{FDR}$ = 0.087). In CNTNAP2$^{-/-}$ mice, overall genotype differences were identified in small clusters in the ventral striatum and ventral hippocampus. A genotype × age interaction was found in ventral striatum with a mixed linear model; pairwise analysis revealed an increase of ventral striatal connectivity in CNTNAP2$^{-/-}$ mice compared with littermates only during adulthood (P$_{FDR}$ = 0.038). In the ventral hippocampus, the strength of network connectivity was reduced at all time points, although it did not survive FDR correction for multiple comparisons (P$_{FDR}$ = 0.062). The genotype × age interaction almost reached significance (P$_{FDR}$ = 0.053) in anterior cingulate, one of the main nodes comprising the default-mode network in mice (Sforazzini et al. 2014; Zerbi et al. 2015) and an important region for social cognition (Apps et al. 2016). In this case, however, connectivity was reduced in the CNTNAP2$^{-/-}$ compared with nontransgenic littermates at p112 (not shown). Data represent mean ± std. deviation.

To improve our understanding of the biological underpinnings of white matter abnormalities revealed by diffusion weighted imaging, we determined the ultrastructure of callosal axons from electron micrographs at Bregma −2.46 mm in Fmr1$^{-/y}$ and CNTNAP2$^{-/-}$ and their respective littermates (Fig. 5). We segmented the inner and outer axonal areas and calculated their circular equivalent diameters to determine the axon and myelin thickness. We further calculated the G-ratio (i.e., the ratio between the inner axonal diameter to the total outer axonal diameter), which is a robust measure for assessing degree of axonal myelination. We found significantly reduced G-ratios (P < 0.001) in both disease models, Fmr1$^{-/y}$ and CNTNAP2$^{-/-}$ mice, compared to their respective wild-type littermates (Fmr1$^{-/y}$: 0.634 ± 0.005 vs. Fmr1$^{+/y}$: 0.682 ± 0.008 and CNTNAP2$^{-/-}$ 0.607 ± 0.005 vs. CNTNAP2$^{+/+}$ 0.651 ± 0.008). In the CNTNAP2$^{-/-}$ mice this reduction was caused by a reduction in

the axonsize (0.372 ± 0.006 in CNTNAP2$^{-/-}$ and 0.460 ± 0.017 in CNTNAP2$^{+/+}$), while the myelin thickness was unaltered (CNTNAP2$^{+/+}$: 0.121 ± 0.044 vs. CNTNAP2$^{-/-}$: 0.120 ± 0.037). In the Fmr1$^{-/y}$ mice the axon diameter was also reduced (P < 0.001; 0.3904 ± 0.010 vs. 0.4422 ± 0.013 in Fmr1$^{+/y}$), however, the myelin thickness was slightly elevated in the Fmr1$^{-/y}$ mice (0.112 ± 0.003 vs. 0.1026 ± 0.004 in Fmr1$^{+/y}$), which might in fact further exacerbate the G-ratio decrease seen in the Fmr1$^{-/y}$ mice.

Discussion

Previous research in humans and rodent models has led to the hypothesis that variations in ASD risk genes affect different aspects of the brain's development trajectory, resulting in the establishment of aberrant functional and/or structural long-range
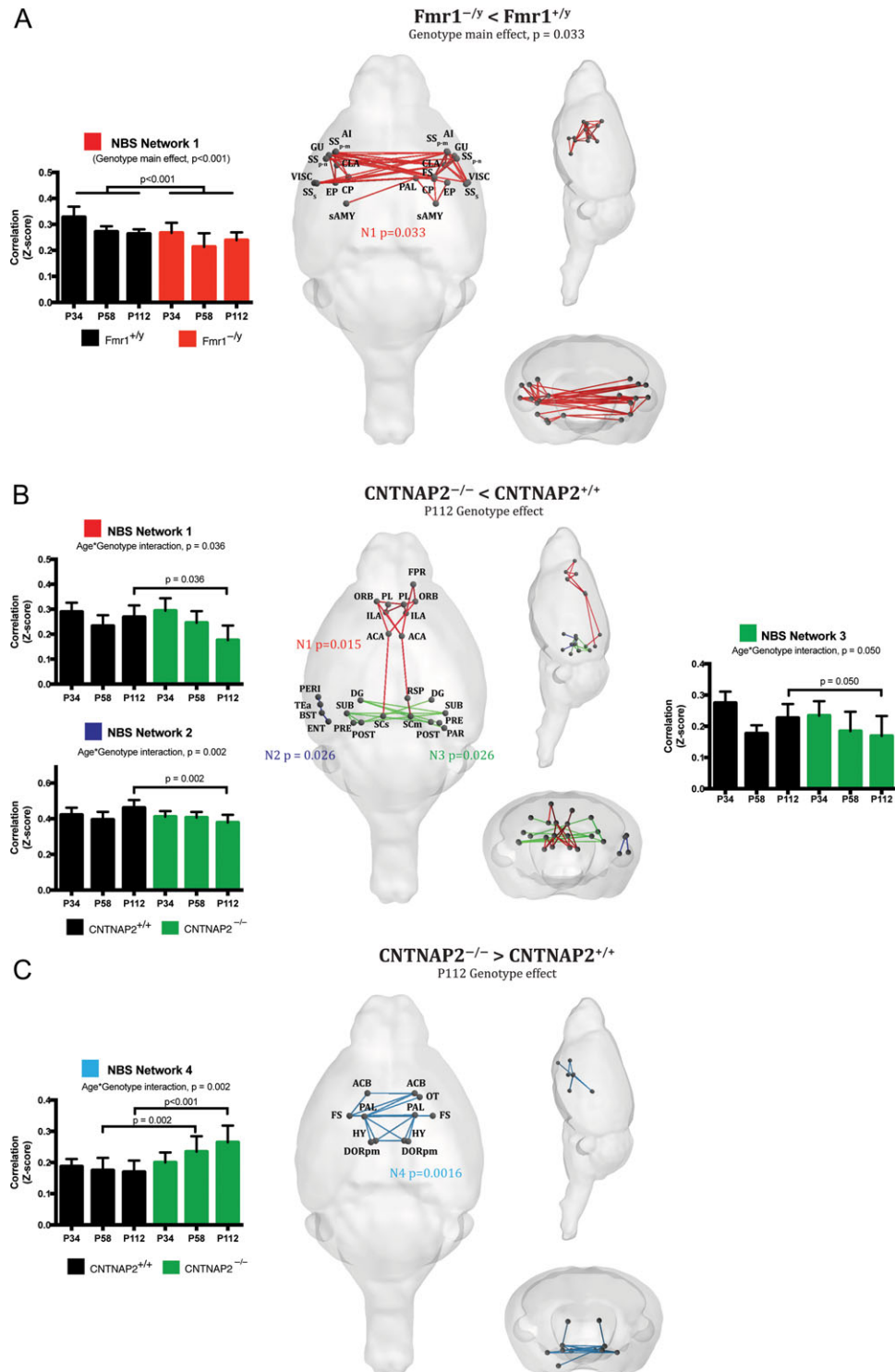
Figure 3. Genotype specific functional connectome analysis. Rs-fMRI connectome analysis combined with network-based statistics (NBS) detected characteristic and distinct pathways of aberrant connectivity in the 2 models. (A) Fmr1$^{-/y}$ mice show severe underconnectivity in bilateral corticocortico and corticostriatal circuits responsible for sensory processing, regardless of age. (B, C) In CNTNAP2$^{-/-}$ mice we detected significant genotype × age interactions in prefrontal-retrosplenial circuits (N1), left associative areas (N2), hippocampus (N3) and ventral striatum-pallidum-hypothalamus (N4). Our analysis shows that under- and overconnectivity profiling are detected only in adult mice, with the exception of the ventral striatum network detected at p58, demonstrating the gradual emergence of circuit-specific pathology over time.

connectivity. Here, we tested this hypothesis by applying longitudinal MRI-based connectivity mapping in 2 knockout mouse models commonly used in ASD research, Fmr1$^{-/y}$ and CNTNAP2$^{-/-}$ mice, during 3 critical developmental periods between childhood

and adulthood. We found deviant functional and structural connectivity in both mouse models though the specific developmental and anatomical pattern depended on the genetic background. Remarkably, we found that from 30 days after birth Fmr1$^{-/y}$ mice
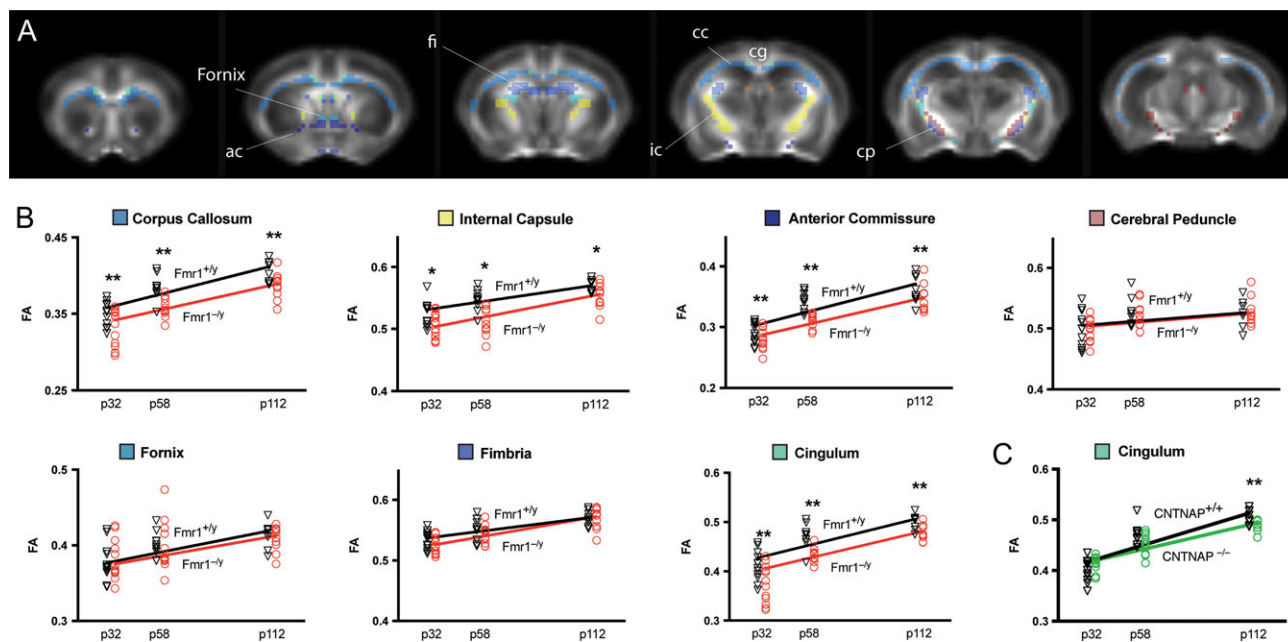
Figure 4. Fractional anisotropy of white matter in Fmr1$^{-/-}$ and CNTNAP2$^{-/-}$ mice. (A) Fractional anisotropy (FA) was assessed by diffusion tensor imaging in Fmr1$^{y/-}$ and CNTNAP2$^{-/-}$ mice and quantified in 7 large white matter structures. (B) At different developmental periods, Fmr1$^{y/-}$ mice had significantly lower FA in 4 major white-matter structures, including corpus callosum, internal capsule, anterior commissure and cingulum. (C) In CNTNAP2$^{-/-}$ an overall reduction of FA was found in the corpus callosum, although it did not survive FDR correction (P$_{FDR}$ = 0.056). However, a strong genotype × age interaction was observed in the cingulum, with a marked reduction of FA only during adulthood. *P$_{FDR}$ < 0.05. **P$_{FDR}$ < 0.01.

exhibited pronounced reduction of functional coupling between sensory-processing areas, indicating that the developmental delay occurred during early childhood. By contrast, CNTNAP2$^{-/-}$ mice developed gradually deviating connectivity patterns in prefrontal and ventral striatal areas between adolescence and adulthood suggesting that related phenotypes became increasingly pronounced later in life. Interestingly, the time point of the aberrant functional and structural connectivity coincides with the expression profile of the knockout genes, suggesting that the timing in which ASD risk-genes are functionally active is critical for the development of aberrant connectivity patterns and possibly behavioral symptoms later in life. The conduction velocity of nerve fibers is influenced by the myelin and axon thickness. Thicker axonal diameters trigger thickening of myelin sheaths and elongation of the internodal segment and therefore lead to an increased internodal conduction velocity of action potentials. We conclude that the overlap of both disease models is a reduced G-ratio and a reduced axon diameter, which could impact the internodal conduction velocity and the overall reliability in signal transmission.

This work supports the growing notion that genetic etiologies may affect different phenotypes and brain circuits (Ellegood et al. 2015; Connor et al. 2016; Huang et al. 2016; Wang et al. 2016). In addition, we emphasize that measuring the developmental trajectory of functional connectivity deficits in ASD models is useful to understand the factors driving the pathology progress and may be crucial when planning a treatment approach.

Functional and Structural Changes in Fmr1 Knockout are Anatomically Located in Brain Areas Processing Sensory Information and are Detectable at a Young Age

Fragile X syndrome (FXS) is the most common syndromic form of ASD, with an estimated 25–50% of children diagnosed with FXS meeting the criteria for ASD (Klusek et al. 2014). Although FXS

represents only a small fraction (~2%) of ASD patients, work on FXS has been particularly beneficial for improving our understanding of ASD. Indeed, FXS and ASD are intertwined at the molecular level (Parikshak et al. 2013), suggesting that several common pathways and cellular mechanisms are shared amongst these 2 disorders. Abnormal methylation of the fragile X mental retardation 1 (FMR1) gene observed in FXS patients leads to a complete or partial absence of fragile-X mental retardation protein (FMRP) (Pieretti et al. 1991). FMRP is highly expressed in the brain and acts as translational repressor of several signaling pathways at the synaptic level (Willemsen et al. 2011). Specifically, FMRP is required for the normal developmental progression of synaptic maturation, and loss of this important RNA binding protein impacts on synaptic plasticity in late embryonic stages and during the first postnatal days (Harlow et al. 2010). Behavioral symptoms include tactile defensiveness, sensory avoidance, and enhanced responses to stimuli of various sensory modalities (Rotschafer and Razak 2014). Symptom severity was found to correlate both with FMR1 activity and FMRP levels (Tassone et al. 1999; Dyer-Friedman et al. 2002; Loesch et al. 2004). As such, hypersensitivity to sensory stimuli—one of the most prominent features of FXS and ASD patients (Baron-Cohen et al. 2009; Gallagher and Hallahan 2012)—has been also described in Fmr1$^{-/y}$ mice (Rotschafer and Razak 2013; Zhang et al. 2014). This defect has been recently attributed to reduced and dysfunctional dendritic ion channels (Zhang et al. 2014), which alters the excitation/inhibition ratio in areas processing sensory information and affects neural plasticity in early postnatal developmental periods (Gibson et al. 2008; Goncalves et al. 2013). Compatible with an earlier study on functional connectivity in Fmr1$^{-/y}$ mice (Haberl, Zerbi, et al. 2015), our data show that the absence of FMRP translates into a hypoconnectivity phenotype at the network level. Thanks to our novel whole-brain data-driven approach, we found this effect specifically for brain networks and pathways associated with sensorial processing and perception (i.e., somatosensory–striatal connections) with strong analogies to symptoms
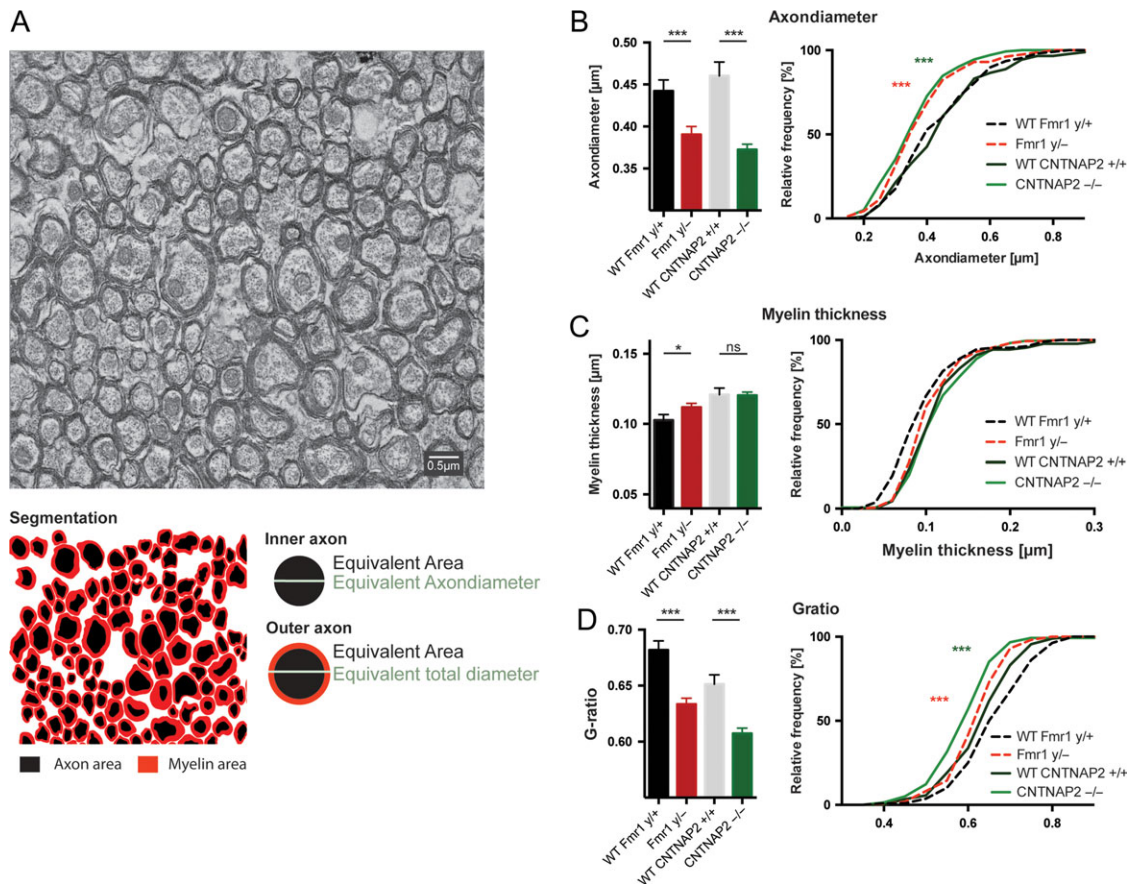
Figure 5. Electron micrograph. (A) Electron micrograph of axons in the corpus callosum. (B) Both, the Fmr1$^{-/y}$ and the CNTNAP2$^{-/-}$ animals have a smaller axon diameter compared with their respective wildtype littermates; the axon diameter distribution confirmed a shift towards smaller axon sizes (KS test). (C) Only minor changes were seen in myelin thickness between the groups, with the Fmr1$^{-/y}$ showing a slight increase compared with their wildtype littermates; however, there were no differences in their cumulative distribution. (D) Both, the Fmr1$^{-/y}$ and the CNTNAP2$^{-/-}$ animals show significant lower G-ratio, calculated as the ratio of the outer to inner equivalent axonal diameters and differ significantly in their distribution (KS test). with a shift towards axons with lower G-ratios. Data represent mean ± standard error.

typical for human FXS patients (Hall et al. 2013; Wilson 2014; Reig and Silberberg 2016). These findings were robust and consistent from 30 days after birth until adulthood, and were observed in both network-based and region-of-interest analyses. Reduction of functional connectivity was paralleled by structural deficits, with DWI revealing severe fiber coherence reductions in corticocortico and corticostriatal pathways. Our finding of lower FA values, which are also often observed in FXS patients (Grigsby 2016), reflect a reduction in axial diffusivity. Further, with electron microscopy we were able to show that the reduction in axial diffusivity was related to a reduction in the inner diameter of the axons, unveiling the microstructural basis for the aberrant functional connectivity patterns.

CNTNAP2 Knockout Mice Display Dysregulation of Connectivity in Prefrontal Cortical Areas

CNTNAP2 is a member of the Neurexin superfamily of transmembrane molecules and affects neuron-glia interactions, thus modulating brain connectivity during early brain maturation. In this neurodevelopmental phase, Caspr2, the protein encoded by CNTNAP2, is thought to assist in interactions important for cellular migration and subsequent laminar organization, indicating a role for CNTNAP2 in the construction of neural circuits (Strauss et al. 2006). CNTNAP2 has been identified as an ASD

risk gene affecting primarily frontal lobe connectivity (Arking et al. 2008; Scott-Van Zeeland et al. 2010). CNTNAP2-KO mice have a reduced number of GABAergic interneurons and impaired migration of cortical projection neurons, which likely cause a higher incidence of seizures and abnormal behaviors such as impaired social interactions and elevated repetitive self-grooming (Penagarikano et al. 2011). In line with these previous observations and a recent functional study (Liska et al. 2017), we report here that the absence of the CNTNAP2 gene is associated with an underconnectivity profile in hippocampal and cortical prefrontal areas linked to reward-guided behavior (Rushworth et al. 2011; Neubert et al. 2015), which match earlier reports in subjects with the CNTNAP2 polymorphism (Scott-Van Zeeland et al. 2010; Dennis et al. 2011). In our connectome analysis, we found that the strongest age-dependent reduction in functional connectivity occurred between nodes that are part of the rodent default-mode network (DMN) (i.e., orbitofrontal, anterior cingulate, and retrosplenial cortices) (Lu et al. 2012; Zerbi et al. 2015; Gozzi and Schwarz 2016). Deactivation of the brain's DMN is often regarded as suppression of endogenous activity to support exogenous task-related processes (Hu et al. 2013). At the same time, reduced activation of the DMN during rest has been associated with a series of pathological conditions, including ASD. Interestingly, in children with ASD, internodal DMN functional connectivity failed to develop during

adolescence (11–13 years) but not during childhood (6–9 years) (Washington et al. 2014). In line with these observations, our results indicate that the connectivity deficits in CNTNAP2$^{-/-}$ mice within the DMN occur as a result of a lack of developmental strengthening of connectivity within this network during adolescence. These findings support the "developmental disconnection model" of the DMN in ASD, which could be related to the reduced number of GABAergic interneurons in these same regions (Scott-Van Zeeland et al. 2010) However, despite sharing some common structural/functional properties (Stafford et al. 2014), there is still no general agreement upon the functional role of this network as a real homologue to the human DMN. Therefore, the translational aspect of these results in the human condition should be taken carefully.

In CNTNAP2$^{-/-}$ mice, we also observed an increase functional coupling between several nodes of the ventral striatum. The ventral striatum is a complex structure that receives and integrates projections from several midbrain regions and across different neurotransmitter systems, including dopamine from ventral tegmental area and substantia nigra, oxytocin from the periventricular nucleus of hypothalamus and noradrenaline from locus coeruleus. In humans, increase functional connectivity between nodes of the ventral striatum has been reported in addiction, anxiety, lack of social motivation, and even obsessive-compulsive disorder (OCD) (Harrison et al. 2009; Sakai et al. 2011; Caldwell 2012). Both OCD and addiction have been related to nucleus accumbens dysfunction during reward processing (Figee et al. 2011; Hommer et al. 2011). Recent studies using optogenetic stimulation found that also frontal cortical areas play a key role in top-down modulation of striatal response to dopaminergic stimuli (Ferenczi et al. 2016). Thus, while activation of the prefrontal cortex and ventral striatum is related to healthy reward processing (Knutson et al. 2001), the disrupted prefrontal coupling and increased connectivity between ventral striatum/pallidum areas found in adult CNTNAP2$^{-/-}$ mice may reflect a shift from healthy goal-directed behavior towards compulsive habits. Although our experiment cannot prove a direct cause–effect relationship, we have shown a time-dependent relationship between the altered connectivity in prefrontal and ventral striatal networks that may be related to the imbalanced excitation/inhibition in mPFC of CNTNAP2$^{-/-}$ mice (Selimbeyoglu et al. 2017).

Notably, we found that deficits in these specific brain circuits gradually emerge during postnatal development and are observable only during adulthood. This age-dependent effect was also found in our structural data, in which a reduction of fiber coherence in the cingulum was observed in adult CNTNAP2 mice compared with wildtype littermates. Anatomically, this single observation is particularly interesting, as it strengthens the idea that structural and functional deficits in these mice primarily affect the limbic system. Furthermore, in CNTNAP2$^{-/-}$ mice we found a reduction in the axonal inner diameter in the corpus callosum, suggesting the presence of an underlying white-matter pathology. Taken together, these data strongly indicate a role for CNTNAP2 in shaping connectivity, particularly between areas of the limbic system, which may have important implications for the appearance of ASD-like behavioral features later in life (Penagarikano and Geschwind 2012).

Interpretational Issues

Measuring brain structural and functional connectivity in mice has high translational value, but both conceptual and methodological interpretational issues may arise when generalizing these findings to the human condition. At the conceptual level, it is unclear how the functional architecture of the mouse brain relates to functional circuits of the human brain. However, in recent years a number of studies have emerged demonstrating rodent–human analogies for basic structural and functional proprieties in networks of high translational importance, such as the default-mode network (Stafford et al. 2014) and striatocortical circuits (Balleine and O'Doherty 2010). While more work needs to be done in this direction, it is envisaged that connectivity measurements may serve the role of an important bridging measurement between human and rodent models, enabling predictions about how specific genetic and molecular alterations observed in mice might be expressed in macroscopic measurements that can be performed in humans (Stafford et al. 2014).

At the methodological level, it is important to consider that our results were collected in a lightly anesthetized state. As previously demonstrated in rats (Bettinardi et al. 2015) and monkeys (Barttfeld et al. 2015), modulating the depth of anesthesia correlates with changes in BOLD variability and reduces the overall connectivity strength. Thus, data acquired with any level of anesthesia cannot be fully generalized to the awake state, although it may have the positive effect of removing confounding BOLD fluctuation due to the environment or unconstrained cognitive shifts while awake. In this study, we took several measures to ensure that the levels of anesthesia were kept as consistent and low as possible, that is, we used mechanical ventilation to maintain the same tidal volume and blood oxygenation throughout the experiment, combined with continuous intravenous infusion of medetomidine and low dose of isoflurane (0.5%), optimized from our previous studies (Grandjean et al. 2014). This allowed us to overcome issues related to high-dose medetomidine (Akeju et al. 2014) and isoflurane accumulation over time (Chuang and Nasrallah 2017). With this protocol, we previously demonstrated that bilateral brain networks are readily detected as compared with other anesthesia protocols (Grandjean et al. 2014) and resemble the anatomical connectome obtained with viral tracer data, up to 90% for corticocortico and corticostriatal circuits (Grandjean et al. 2017). The light-anesthesia regime also minimizes the possibility that the mapped changes are the results of different brain states reflecting genotype-dependent sensitivity to anesthesia, as it was previously suggested for Fmr1$^{-/y}$ mice (Goncalves et al. 2013). Importantly, our results show functional connectivity defects in both Fmr1$^{-/y}$ and CNTNAP2$^{-/-}$ mice that are circuit-specific. A higher or lower sensitivity to the anesthesia in one group would have instead resulted in an increased or reduced connectivity in all the identified networks or pathways. Furthermore, our results are consistent with 2 other independent studies, which used different anesthesia setups (isoflurane-only and urethane). Because these agents act on different neurotransmitter systems (Hara and Harris 2002; Chuang and Nasrallah 2017) it is unlikely that common genotype × anesthesia effects would fully explain the findings of both studies. Finally, we present evidence that functional deficits are paired with structural deficits in the same anatomical locations, either by viral tracer, EM, or diffusion data.

It is important to mention that all between-groups comparisons were performed between matched strain-, age-, gender-, and bodyweight conditions; this experimental design is of critical importance to avoid confounding systematic variations in rs-fMRI parameters. Given that the physiological (and statistically significant) increase in bodyweight over time may systematically confound the anesthesia dosage, here we took a conservative position when interpreting effects arising from changes of rs-fMRI parameters as a function of age.

Conclusions

MRI-based connectivity mapping has become the method of choice for investigating hyperconnected and hypoconnected pathways at the systems level and across the whole brain. Applied to a suitable disease model system such as the mouse, it turns into a powerful translational tool to study gene-to-neural circuits interactions while minimizing the influence of environmental heterogeneity. In this study, we investigated developmental changes in 2 animal models for ASD. We demonstrated that mutations in ASD risk genes, which are known to alter cell and synaptic functioning, cause aberrant structural and functional connectivity within specific circuits. We also show that deviations from the normal developmental trajectory might be powerful markers of ASD, though the genetic background determines at which time point such deviations manifest themselves. Interestingly, these time points appear to correspond to the temporal expression profile of proteins encoded by the affected gene. The anatomical specificity of our measurements allowed for the detection of robust group-level brain connectivity profiles that can act as "fingerprints" to accurately identify the genetic contribution to the connectome shape and strength, and opens new perspectives for using this technique as a translational tool between animal models and humans. In summary, our results provide important evidence that measuring developmental changes in the functional and structural brain architecture using neuroimaging might reveal disease markers of clinical utility.

Supplementary Material

Supplementary material is available at *Cerebral Cortex* online.

Funding

Notes

References

Abraham A, Milham MP, Di Martino A, Craddock RC, Samaras D, Thirion B, Varoquaux G. 2017. Deriving reproducible biomarkers from multi-site resting-state data: an autism-based example. Neuroimage. 147:736–745.

Akeju O, Loggia ML, Catana C, Pavone KJ, Vazquez R, Rhee J, Contreras Ramirez V, Chonde DB, Izquierdo-Garcia D, Arabasz G, et al. 2014. Disruption of thalamic functional connectivity is a neural correlate of dexmedetomidine-induced unconsciousness. Elife. 3:e04499.

Alaerts K, Geerlings F, Herremans L, Swinnen SP, Verhoeven J, Sunaert S, Wenderoth N. 2015. Functional organization of the action observation network in autism: a graph theory approach. PLoS One. 10:e0137020.

Alaerts K, Swinnen SP, Wenderoth N. 2016. Sex differences in autism: a resting-state fMRI investigation of functional brain connectivity in males and females. Soc Cogn Affect Neurosci. 11:1002–1016.

Alaerts K, Woolley DG, Steyaert J, Di Martino A, Swinnen SP, Wenderoth N. 2014. Underconnectivity of the superior temporal sulcus predicts emotion recognition deficits in autism. Soc Cogn Affect Neurosci. 9:1589–1600.

Apps MA, Rushworth MF, Chang SW. 2016. The anterior cingulate gyrus and social cognition: tracking the motivation of others. Neuron. 90:692–707.

Arking DE, Cutler DJ, Brune CW, Teslovich TM, West K, Ikeda M, Rea A, Guy M, Lin S, Cook EH, et al. 2008. A common genetic variant in the neurexin superfamily member CNTNAP2 increases familial risk of autism. Am J Hum Genet. 82:160–164.

Balleine BW, O'Doherty JP. 2010. Human and rodent homologies in action control: corticostriatal determinants of goal-directed and habitual action. Neuropsychopharmacology. 35:48–69.

Balsters JH, Apps MA, Bolis D, Lehner R, Gallagher L, Wenderoth N. 2017. Disrupted prediction errors index social deficits in autism spectrum disorder. Brain. 140:235–246.

Balsters JH, Mantini D, Apps MA, Eickhoff SB, Wenderoth N. 2016. Connectivity-based parcellation increases network detection sensitivity in resting state fMRI: an investigation into the cingulate cortex in autism. Neuroimage Clin. 11:494–507.

Balsters JH, Mantini D, Wenderoth N. 2017. Connectivity-based parcellation reveals distinct cortico-striatal connectivity fingerprints in Autism Spectrum Disorder. Neuroimage. pii: S1053-8119(17)30123-4 [Epub ahead of print].

Baron-Cohen S, Ashwin E, Ashwin C, Tavassoli T, Chakrabarti B. 2009. Talent in autism: hyper-systemizing, hyper-attention to detail and sensory hypersensitivity. Philos Trans R Soc Lond B Biol Sci. 364:1377–1383.

Barttfeld P, Uhrig L, Sitt JD, Sigman M, Jarraya B, Dehaene S. 2015. Signature of consciousness in the dynamics of resting-state brain activity. Proc Natl Acad Sci USA. 112:887–892.

Belmonte MK, Allen G, Beckel-Mitchener A, Boulanger LM, Carper RA, Webb SJ. 2004. Autism and abnormal development of brain connectivity. J Neuroscience. 24:9228–9231.

Bettinardi RG, Tort-Colet N, Ruiz-Mejias M, Sanchez-Vives MV, Deco G. 2015. Gradual emergence of spontaneous correlated brain activity during fading of general anesthesia in rats: evidences from fMRI and local field potentials. Neuroimage. 114:185–198.

Caldwell HK. 2012. Neurobiology of sociability. Adv Exp Med Biol. 739:187–205.

Chuang KH, Nasrallah FA. 2017. Functional networks and network perturbations in rodents. Neuroimage. 163:419–436.

Connor SA, Ammendrup-Johnsen I, Chan AW, Kishimoto Y, Murayama C, Kurihara N, Tada A, Ge Y, Lu H, Yan R, et al. 2016. Altered cortical dynamics and cognitive function upon haploinsufficiency of the autism-linked excitatory synaptic suppressor MDGA2. Neuron. 91:1052–1068.

Courchesne E. 2002. Abnormal early brain development in autism. Mol Psychiatry. 7(Suppl 2):S21–S23.

Dennis EL, Jahanshad N, Rudie JD, Brown JA, Johnson K, McMahon KL, de Zubicaray GI, Montgomery G, Martin NG, Wright MJ, et al. 2011. Altered structural brain connectivity

in healthy carriers of the autism risk gene, CNTNAP2. Brain Connect. 1:447–459.

Dyer-Friedman J, Glaser B, Hessl D, Johnston C, Huffman LC, Taylor A, Wisbeck J, Reiss AL. 2002. Genetic and environmental influences on the cognitive outcomes of children with fragile X syndrome. J Am Acad Child Adolesc Psychiatry. 41:237–244.

Ellegood J, Anagnostou E, Babineau BA, Crawley JN, Lin L, Genestine M, DiCicco-Bloom E, Lai JK, Foster JA, Penagarikano O, et al. 2015. Clustering autism: using neuroanatomical differences in 26 mouse models to gain insight into the heterogeneity. Mol Psychiatry. 20:118–125.

Ferenczi EA, Zalocusky KA, Liston C, Grosenick L, Warden MR, Amatya D, Katovich K, Mehta H, Patenaude B, Ramakrishnan C, et al. 2016. Prefrontal cortical regulation of brainwide circuit dynamics and reward-related behavior. Science. 351:aac9698.

Figee M, Vink M, de Geus F, Vulink N, Veltman DJ, Westenberg H, Denys D. 2011. Dysfunctional reward circuitry in obsessive-compulsive disorder. Biol Psychiatry. 69:867–874.

Filippini N, MacIntosh BJ, Hough MG, Goodwin GM, Frisoni GB, Smith SM, Matthews PM, Beckmann CF, Mackay CE. 2009. Distinct patterns of brain activity in young carriers of the APOE-epsilon4 allele. Proc Natl Acad Sci USA. 106:7209–7214.

Gallagher A, Hallahan B. 2012. Fragile X-associated disorders: a clinical overview. J Neurol. 259:401–413.

Garcia-Pino E, Gessele N, Koch U. 2017. Enhanced excitatory connectivity and disturbed sound processing in the auditory brainstem of fragile X mice. J Neurosci. 37:7403–7419.

Gibson JR, Bartley AF, Hays SA, Huber KM. 2008. Imbalance of neocortical excitation and inhibition and altered UP states reflect network hyperexcitability in the mouse model of fragile X syndrome. J Neurophysiol. 100:2615–2626.

Goncalves JT, Anstey JE, Golshani P, Portera-Cailliau C. 2013. Circuit level defects in the developing neocortex of fragile X mice. Nat Neurosci. 16:903–909.

Gozzi A, Schwarz AJ. 2016. Large-scale functional connectivity networks in the rodent brain. Neuroimage. 127:496–509.

Grandjean J, Schroeter A, Batata I, Rudin M. 2014. Optimization of anesthesia protocol for resting-state fMRI in mice based on differential effects of anesthetics on functional connectivity patterns. Neuroimage. 102(Pt 2):838–847.

Grandjean J, Zerbi V, Balsters JH, Wenderoth N, Rudin M. 2017. Structural basis of large-scale functional connectivity in the mouse. J Neurosci. 37:8092–8101.

Grigsby J. 2016. The fragile X mental retardation 1 gene (FMR1): historical perspective, phenotypes, mechanism, pathology, and epidemiology. Clin Neuropsychol. 30:815–833.

Haberl MG, Ginger M, Frick A. 2017. Dual anterograde and retrograde viral tracing of reciprocal connectivity. Methods Mol Biol. 1538:321–340.

Haberl MG, Viana da Silva S, Guest JM, Ginger M, Ghanem A, Mulle C, Oberlaender M, Conzelmann KK, Frick A. 2015. An anterograde rabies virus vector for high-resolution large-scale reconstruction of 3D neuron morphology. Brain Struct Funct. 220:1369–1379.

Haberl MG, Zerbi V, Veltien A, Ginger M, Heerschap A, Frick A. 2015. Structural-functional connectivity deficits of neocortical circuits in the Fmr1 (–/y) mouse model of autism. Sci Adv. 1: e1500775.

Hagerman RJ, Hagerman P. 2016. Fragile X-associated tremor/ataxia syndrome—features, mechanisms and management. Nat Rev Neurol. 12:403–412.

Hall SS, Jiang H, Reiss AL, Greicius MD. 2013. Identifying large-scale brain networks in fragile X syndrome. JAMA Psychiatry. 70:1215–1223.

Hara K, Harris RA. 2002. The anesthetic mechanism of urethane: the effects on neurotransmitter-gated ion channels. Anesth Analg. 94:313–318. , table of contents.

Harada M, Taki MM, Nose A, Kubo H, Mori K, Nishitani H, Matsuda T. 2011. Non-invasive evaluation of the GABAergic/glutamatergic system in autistic patients observed by MEGA-editing proton MR spectroscopy using a clinical 3 tesla instrument. J Autism Dev Disord. 41:447–454.

Harlow EG, Till SM, Russell TA, Wijetunge LS, Kind P, Contractor A. 2010. Critical period plasticity is disrupted in the barrel cortex of FMR1 knockout mice. Neuron. 65:385–398.

Harrison BJ, Soriano-Mas C, Pujol J, Ortiz H, Lopez-Sola M, Hernandez-Ribas R, Deus J, Alonso P, Yucel M, Pantelis C, et al. 2009. Altered corticostriatal functional connectivity in obsessive-compulsive disorder. Arch Gen Psychiatry. 66:1189–1200.

Hashemi E, Ariza J, Rogers H, Noctor SC, Martinez-Cerdeno V. 2017. The number of parvalbumin-expressing interneurons is decreased in the medial prefrontal cortex in autism. Cereb Cortex. 27:1931–1943.

Hashimoto R, Srivastava S, Tassone F, Hagerman RJ, Rivera SM. 2011. Diffusion tensor imaging in male premutation carriers of the fragile X mental retardation gene. Mov Disord. 26: 1329–1336.

Hazlett HC, Gu H, Munsell BC, Kim SH, Styner M, Wolff JJ, Elison JT, Swanson MR, Zhu H, Botteron KN, et al, IBIS Network; Clinical Sites; Data Coordinating Center; Image Processing Core; Statistical Analysis. 2017. Early brain development in infants at high risk for autism spectrum disorder. Nature. 542:348–351.

Hinds HL, Ashley CT, Sutcliffe JS, Nelson DL, Warren ST, Housman DE, Schalling M. 1993. Tissue specific expression of FMR-1 provides evidence for a functional role in fragile X syndrome. Nat Genet. 3:36–43.

Hommer DW, Bjork JM, Gilman JM. 2011. Imaging brain response to reward in addictive disorders. Ann NY Acad Sci. 1216:50–61.

Hu Y, Chen X, Gu H, Yang Y. 2013. Resting-state glutamate and GABA concentrations predict task-induced deactivation in the default mode network. J Neurosci. 33:18566–18573.

Huang WC, Chen Y, Page DT. 2016. Hyperconnectivity of prefrontal cortex to amygdala projections in a mouse model of macrocephaly/autism syndrome. Nat Commun. 7:13421.

Kassraian-Fard P, Matthis C, Balsters JH, Maathuis MH, Wenderoth N. 2016. Promises, pitfalls, and basic guidelines for applying machine learning classifiers to psychiatric imaging data, with autism as an example. Front Psychiatry. 7:177.

Klusek J, Martin GE, Losh M. 2014. Consistency between research and clinical diagnoses of autism among boys and girls with fragile X syndrome. J Intellect Disabil Res. 58:940–952.

Knutson B, Fong GW, Adams CM, Varner JL, Hommer D. 2001. Dissociation of reward anticipation and outcome with event-related fMRI. Neuroreport. 12(17):3683–3687.

Lebel C, Walker L, Leemans A, Phillips L, Beaulieu C. 2008. Microstructural maturation of the human brain from childhood to adulthood. Neuroimage. 40:1044–1055.

Lee E, Lee J, Kim E. 2017. Excitation/inhibition imbalance in animal models of autism spectrum disorders. Biol Psychiatry. 81:838–847.

Liska A, Bertero A, Gomolka R, Sabbioni M, Galbusera A, Barsotti N, Panzeri S, Scattoni ML, Pasqualetti M, Gozzi A. 2017. Homozygous loss of autism-risk gene CNTNAP2 results in reduced local and long-range prefrontal functional connectivity. Cereb Cortex. doi: 10.1093/cercor/bhx022. [Epub ahead of print].

Loesch DZ, Huggins RM, Hagerman RJ. 2004. Phenotypic variation and FMRP levels in fragile X. Ment Retard Dev Disabil Res Rev. 10:31–41.

Lu H, Zou Q, Gu H, Raichle ME, Stein EA, Yang Y. 2012. Rat brains also have a default mode network. Proc Natl Acad Sci USA. 109:3979–3984.

Mientjes EJ, Nieuwenhuizen I, Kirkpatrick L, Zu T, Hoogeveen-Westerveld M, Severijnen L, Rife M, Willemsen R, Nelson DL, Oostra BA. 2006. The generation of a conditional Fmr1 knock out mouse model to study Fmrp function in vivo. Neurobiol Dis. 21:549–555.

Neubert FX, Mars RB, Sallet J, Rushworth MF. 2015. Connectivity reveals relationship of brain areas for reward-guided learning and decision making in human and monkey frontal cortex. Proc Natl Acad Sci USA. 112:E2695–E2704.

Oh SW, Harris JA, Ng L, Winslow B, Cain N, Mihalas S, Wang Q, Lau C, Kuan L, Henry AM, et al. 2014. A mesoscale connectome of the mouse brain. Nature. 508:207–214.

Parikshak NN, Luo R, Zhang A, Won H, Lowe JK, Chandran V, Horvath S, Geschwind DH. 2013. Integrative functional genomic analyses implicate specific molecular pathways and circuits in autism. Cell. 155:1008–1021.

Patel AX, Kundu P, Rubinov M, Jones PS, Vertes PE, Ersche KD, Suckling J, Bullmore ET. 2014. A wavelet method for modeling and despiking motion artifacts from resting-state fMRI time series. Neuroimage. 95:287–304.

Penagarikano O, Abrahams BS, Herman EI, Winden KD, Gdalyahu A, Dong H, Sonnenblick LI, Gruver R, Almajano J, Bragin A, et al. 2011. Absence of CNTNAP2 leads to epilepsy, neuronal migration abnormalities, and core autism-related deficits. Cell. 147:235–246.

Penagarikano O, Geschwind DH. 2012. What does CNTNAP2 reveal about autism spectrum disorder? Trends Mol Med. 18:156–163.

Pieretti M, Zhang FP, Fu YH, Warren ST, Oostra BA, Caskey CT, Nelson DL. 1991. Absence of expression of the FMR-1 gene in fragile X syndrome. Cell. 66:817–822.

Reig R, Silberberg G. 2016. Distinct corticostriatal and intracortical pathways mediate bilateral sensory responses in the striatum. Cereb Cortex. 26:4405–4415.

Ronald A, Hoekstra RA. 2011. Autism spectrum disorders and autistic traits: a decade of new twin studies. Am J Med Genet B Neuropsychiatr Genet. 156B:255–274.

Rotschafer S, Razak K. 2013. Altered auditory processing in a mouse model of fragile X syndrome. Brain Res. 1506: 12–24.

Rotschafer SE, Razak KA. 2014. Auditory processing in fragile x syndrome. Front Cell Neurosci. 8:19.

Rubenstein JL, Merzenich MM. 2003. Model of autism: increased ratio of excitation/inhibition in key neural systems. Genes, Brain Behav. 2:255–267.

Rushworth MF, Noonan MP, Boorman ED, Walton ME, Behrens TE. 2011. Frontal cortex and reward-guided learning and decision-making. Neuron. 70:1054–1069.

Sakai Y, Narumoto J, Nishida S, Nakamae T, Yamada K, Nishimura T, Fukui K. 2011. Corticostriatal functional connectivity in non-medicated patients with obsessive-compulsive disorder. Eur Psychiatry. 26:463–469.

Scott-Van Zeeland AA, Abrahams BS, Alvarez-Retuerto AI, Sonnenblick LI, Rudie JD, Ghahremani D, Mumford JA, Poldrack RA, Dapretto M, Geschwind DH, et al. 2010. Altered functional connectivity in frontal lobe circuits is associated with variation in the autism risk gene CNTNAP2. Sci Transl Med. 2:56ra80.

Selimbeyoglu A, Kim CK, Inoue M, Lee SY, Hong ASO, Kauvar I, Ramakrishnan C, Fenno LE, Davidson TJ, Wright M, et al. 2017. Modulation of prefrontal cortex excitation/inhibition balance rescues social behavior in CNTNAP2-deficient mice. Sci Transl Med. 9:eaah6733.

Sethi SS, Zerbi V, Wenderoth N, Fornito A, Fulcher BD. 2017. Structural connectome topology relates to regional BOLD signal dynamics in the mouse brain. Chaos. 27:047405.

Sforazzini F, Schwarz AJ, Galbusera A, Bifone A, Gozzi A. 2014. Distributed BOLD and CBV-weighted resting-state networks in the mouse brain. Neuroimage. 87:403–415.

Stafford JM, Jarrett BR, Miranda-Dominguez O, Mills BD, Cain N, Mihalas S, Lahvis GP, Lattal KM, Mitchell SH, David SV, et al. 2014. Large-scale topology and the default mode network in the mouse connectome. Proc Natl Acad Sci USA. 111: 18745–18750.

Strauss KA, Puffenberger EG, Huentelman MJ, Gottlieb S, Dobrin SE, Parod JM, Stephan DA, Morton DH. 2006. Recessive symptomatic focal epilepsy and mutant contactin-associated protein-like 2. N Engl J Med. 354:1370–1377.

Tassone F, Hagerman RJ, Ikle DN, Dyer PN, Lampe M, Willemsen R, Oostra BA, Taylor AK. 1999. FMRP expression as a potential prognostic indicator in fragile X syndrome. Am J Med Genet. 84:250–261.

Vasa RA, Mostofsky SH, Ewen JB. 2016. The disrupted connectivity hypothesis of autism spectrum disorders: time for the next phase in research. Biol Psychiatry Cogn Neurosci Neuroimaging. 1:245–252.

Wang X, Bey AL, Katz BM, Badea A, Kim N, David LK, Duffney LJ, Kumar S, Mague SD, Hulbert SW, et al. 2016. Altered mGluR5-Homer scaffolds and corticostriatal connectivity in a Shank3 complete knockout model of autism. Nat Commun. 7:11459.

Washington SD, Gordon EM, Brar J, Warburton S, Sawyer AT, Wolfe A, Mease-Ference ER, Girton L, Hailu A, Mbwana J, et al. 2014. Dysmaturation of the default mode network in autism. Hum Brain Mapp. 35:1284–1296.

Willemsen R, Levenga J, Oostra BA. 2011. CGG repeat in the FMR1 gene: size matters. Clin Genet. 80:214–225.

Wilson CJ. 2014. The sensory striatum. Neuron. 83:999–1001.

Yizhar O, Fenno LE, Prigge M, Schneider F, Davidson TJ, O'Shea DJ, Sohal VS, Goshen I, Finkelstein J, Paz JT, et al. 2011. Neocortical excitation/inhibition balance in information processing and social dysfunction. Nature. 477:171–178.

Zalesky A, Fornito A, Bullmore ET. 2010. Network-based statistic: identifying differences in brain networks. Neuroimage. 53:1197–1207.

Zerbi V, Grandjean J, Rudin M, Wenderoth N. 2015. Mapping the mouse brain with rs-fMRI: an optimized pipeline for functional network identification. Neuroimage. 123:11–21.

Zerbi V, Kleinnijenhuis M, Fang X, Jansen D, Veltien A, Van Asten J, Timmer N, Dederen PJ, Kiliaan AJ, Heerschap A. 2013. Gray and white matter degeneration revealed by diffusion in an Alzheimer mouse model. Neurobiol Aging. 34:1440–1450.

Zerbi V, Wiesmann M, Emmerzaal TL, Jansen D, Van Beek M, Mutsaers MP, Beckmann CF, Heerschap A, Kiliaan AJ. 2014. Resting-state functional connectivity changes in aging apoE4 and apoE-KO mice. J Neurosci. 34:13963–13975.

Zhang Y, Bonnan A, Bony G, Ferezou I, Pietropaolo S, Ginger M, Sans N, Rossier J, Oostra B, LeMasson G, et al. 2014. Dendritic channelopathies contribute to neocortical and sensory hyperexcitability in Fmr1(–/y) mice. Nat Neurosci. 17:1701–1709.